Soft Matter

PAPER

View Article Online
View Journal | View Issue

Cite this: *Soft Matter*, 2014, **10**, 9254

Role of shear-induced dynamical heterogeneity in the nonlinear rheology of colloidal gels†

Lilian C. Hsiao,‡§[a] Heekyoung Kang,‡[b] Kyung Hyun Ahn[b] and Michael J. Solomon*[a]

Received 24th June 2014
Accepted 4th October 2014

DOI: 10.1039/c4sm01375a

www.rsc.org/softmatter

We report the effect of flow-induced dynamical heterogeneity on the nonlinear elastic modulus of weakly aggregated colloidal gels that have undergone yielding by an imposed step strain deformation. The gels are comprised of sterically stabilized poly(methyl methacrylate) colloids interacting through short-ranged depletion attractions. When a step strain of magnitude varying from $\gamma = 0.1$ to 80.0 is applied to the quiescent gels, we observe the development of a bimodal distribution in the single-particle van Hove self-correlation function. This distribution is consistent with the existence of a fast and slow subpopulation of colloids within sheared gels. We evaluate the effect of incorporating the properties of the slow, rigid subpopulation of the colloids into a recent mode coupling theory for the nonlinear elasticity of colloidal gels.

Introduction

Weak, reversible colloidal gels are important model systems for studying the underlying physics of attractive interactions, slow dynamics, and yielding transitions. They exhibit structural and dynamical heterogeneity,[1–4] ergodic/nonergodic transitions,[5–8] and complex linear and nonlinear flow properties.[9–11] In contrast to the caging mechanism that gives rise to slow dynamics in dense colloidal suspensions, the elasticity imparted by gels arises from three-dimensional network structures that are assembled by attractive bonding between individual colloids. Mode coupling theory (MCT) has been used to model the dynamics of collective modes of the disordered gel structure.[12,13] A key finding is that the elastic modulus is inversely related to the ensemble-averaged single particle localization length.[12,14–16] While linear rheological experiments show good agreement with the MCT prediction for gels at low volume fractions,[17] significant discrepancies have been observed in certain weak, transient systems.[18] The discrepancy has been attributed to the MCT assumption of a homogenous fluid, in which the large cluster length scales associated with heterogeneous gel structure have been neglected.[19] A prefactor corresponding to the average number of colloids in each cluster has been used to reconcile the theoretical predictions with experimental measurements.[15,18,19]

Structural and dynamical heterogeneity in quiescent gels are correlated, particularly in the cluster regime close to the gelation transition.[3,4,21–23] Heterogeneity can also arise from yielding, where sequences of bond rupture occur beyond a critical applied strain or stress. Nonlinear rheological phenomenon such as shear banding,[24] slip,[25] and strain-induced hardening/softening[26] are often encountered in flows that are sufficiently large to cause yielding. Strong flows perturb the nonequilibrium free energy landscape and affect slow colloidal dynamics in surprising ways.[27] For example, nonergodic clusters exhibit ballistic motion at short time scales,[28] followed by a gradual relaxation of internal stress after flow ceases.[29] Despite the importance of structural and dynamical heterogeneity in microscopic models, experiments have yet to probe the effect of flow on dynamical heterogeneity and its role in the nonlinear rheological behavior of yielded gels. Here, we report experiments that show the existence of strain-induced dynamical heterogeneity in colloidal gels. The dynamical heterogeneity takes a simple form comprised of slow and fast subpopulations of colloids. We show that the predictions from a particular form of MCT, where the local dynamics of the system is characterized by the ensemble-averaged mean squared displacement of the particles, agrees well with experimental measurements of nonlinear elasticity if we hypothesize that only the slow, hydrodynamically rigid subpopulation of colloids contribute to the elastic component of the stress.

Experimental methods

Confocal microscopy imaging of gels under shear

The gels studied are comprised of poly(methyl methacrylate) (PMMA) spheres (diameter, $2a = 900$ nm $\pm$ 6%) sterically

[a]*Department of Chemical Engineering, University of Michigan, MI, USA. E-mail: mjsolo@umich.edu*

[b]*School of Chemical and Biological Engineering, Institute of Chemical Process, Seoul National University, Seoul, 151-744, Korea*

† Electronic supplementary information (ESI) available. See DOI: 10.1039/c4sm01375a

‡ These authors contributed equally to this work.

§ Present address: Department of Chemical Engineering, Massachusetts Institute of Technology, MA, USA.

stabilized with diphenyl-dimethyl siloxane, dyed with fluorescent Nile Red,[2,4] and dispersed in a refractive index and density matched solvent (55/10/35 vol% cyclohexyl bromide/decalin/dioctyl phthalate, $\Delta n = 1.0 \times 10^{-3}$, $\Delta\rho/\rho = 4.0 \times 10^{-3}$). This solvent composition is selected to optimize observation of dynamical changes within experimental time scales (solvent viscosity, $\eta = 2.7 \times 10^{-2}$ Pa s, diffusivity $D = 1.8 \times 10^{-14}$ m^2 s^{-1}). We add non-adsorbing polystyrene (molecular weight = 900 000 g mol^{-1}) where the radius of gyration, $R_g = 38 \pm 2$ nm, is determined by static light scattering (DAWN EOS, Wyatt Technology, 690 nm laser). The small polystyrene molecule is added at a dilute concentration (overlap concentration $c^* = 0.007 \pm 0.001$ g mL^{-1}, $c_{sample} = c/c^* = 0.31 \pm 0.05$) to the PMMA colloids, generating gels with moderate volume fraction ($\phi = 0.15$) and short-ranged attractions ($\xi = R_g/a = 0.08$). The weak, cluster-like gels generated here are close to the onset of gelation at $c_{gel} = c/c^* \sim 0.25$, where $(c_{sample} - c_{gel})/c_{gel} = 0.24$. Tetrabutylammonium chloride is added at a concentration of 1 μM (zeta potential, $\zeta \leq 10$ mV,[2] Debye length, $\kappa^{-1} = 70$ nm) to provide charge screening. The net interparticle potential is estimated at $U \sim (-2.2 \pm 0.5)\ k_BT$ (k_B is the Boltzmann constant, and temperature $T = 298$ K) and is comparable to weak colloidal gels.[4,30]

The dynamics of the gels are monitored at waiting times of t_w = 10 min, 30 min, 1 hour and 2 hours after sample loading. Representative confocal images of the effect of waiting time on the microstructure of these gels are shown in ESI Fig. 1(a)–(d).† The mean-squared displacement (MSD) values and the van Hove self-correlation functions plotted in the figure show that the colloids become increasingly arrested over the course of 2 hours. ESI Fig. 1(e)† shows that the MSD of the gels attain a plateau localization length of $\langle \Delta x^2(\Delta t) \rangle = (6.5 \pm 2.0) \times 10^{-4}$ μm^2 at $t_w = 2$ hours. Similarly, ESI Fig. 1(f)† shows that the single particle displacement probability is narrow and non-Gaussian. These quiescent gels are cluster-like and exhibit non-Gaussian dynamics typical of weakly-aggregated gels,[4] but without a bimodal distribution that is sometimes observed close to the gelation transition.[3,23]

Gel samples are loaded into a custom-built shearing device set at a gap of 120 μm (ref. 2 and 31) and mounted on a confocal laser-scanning microscope (Leica SP2, 100×, 1.4 numerical aperture oil immersion objective). The gels are allowed to rest for 2 hours in the shear cell, and step strains of various magnitudes ($\gamma = 0.1, 0.6, 6.0, 30.0, 80.0$) are applied at a shear rate of 40 s^{-1} (Péclet number, Pe = 1300). The high shear rate is chosen to avoid shear banding.[2] Single particle dynamics of the sheared gels are tracked in two dimensions (2D particle tracking) over a total period of 130 s with a lag time, Δt, of 0.652 s. Particles that are tracked for 20 consecutive frames or more are used for analysis. A small center-of-mass drift of specimens is addressed with a constant velocity correction.[32] Three independent samples are analyzed for each strain, except for $\gamma = 0.6$ where only one replication was available for analysis because of large image center-of-mass drift velocities. The resulting mean-squared displacement (MSD) of sheared gels at each γ is determined with respect to the velocity and vorticity directions of the applied flow. The static error in the MSD sets the lower bound on the MSD due to instrument and environmental fluctuations. A control experiment on an immobile, photopolymerized gel sample establishes this lower bound at 3.20×10^{-4} μm^2. Because of residual flow at the highest strain (γ = 80.0) that is predominantly in the flow direction, we wait up to an additional 5 minutes after the step strain to acquire images in this case, and analyze all single particle dynamics in only the vorticity direction. The self-part of the one-dimensional van Hove correlation function, $G_s(\Delta x, \Delta t) = \frac{1}{N}\left\langle \sum_{i=1}^{N} \delta(x + x_i(t=0) - x_i(t)) \right\rangle$, is used to characterize the probability distribution of single-particle displacements, where N is the total number of particles.

Rheological characterization of the nonlinear elastic modulus after yielding

The nonlinear elastic modulus of the yielded colloidal gels is measured using a stress-controlled rheometer (AR-G2, TA Instruments) with a 40 mm parallel steel plate geometry (gap = 500 μm). A solvent trap is used to minimize evaporation of the volatile solvent. Gels are presheared at 200 rad s^{-1} for 2 minutes and allowed to equilibrate for 2 hours prior to measurements. The strain-dependent elastic modulus, $G'(\gamma)$, is measured using oscillatory stress sweep experiments performed at four different angular frequencies ($\omega = 0.1, 1, 10, 40$ rad s^{-1}, ESI Fig. 2†). The dependence of $G'(\gamma)$ on ω and the relative similarity of the linear elastic and viscous moduli at low γ, G' and G'', show that the gels are weak, consistent with the strength of pair attractions in this system. As a basis for comparison with MCT, which can be used to predict the zero-frequency elastic modulus, we normalize the experimentally measured $G'(\gamma)$ at different ω by the linear plateau value, G' (ESI Fig. 2,† inset).

Results and discussion

Single-particle dynamics of yielded gels

Fig. 1(a) and (b) show representative images of gels imaged at h = 60 μm above the coverslip after applying a small ($\gamma = 0.6$) and large ($\gamma = 80.0$) step strain. While the yielded structures appear visually similar, the dynamical signatures at each applied strain are very different from each other. Fig. 1(c) shows that the application of step strain results in an increase in the one-dimensional MSD, measured in the vorticity direction, $\langle \Delta x^2(\Delta t) \rangle$, relative to the unsheared gels. (We show MSD data for $\Delta t \leq 20.2$ s because both fast and slow populations of the gels can be adequately resolved by the 2D particle tracking in this temporal range.) Quiescent gels exhibit a mean squared localization length at $\langle \Delta x^2(\Delta t) \rangle = (6.5 \pm 2.0) \times 10^{-4}$ μm^2. Over the duration of the measurements for post-yield samples, the MSD is approximately constant, particularly for small step strains (γ = 0.1–30.0). At γ = 80.0, the sheared samples display sub-diffusive motion with a MSD slope power law exponent of 0.75 ± 0.01. The increase in MSD of particles in the sheared gels is an indication that increasing the magnitude of the applied step strain results in increased delocalization of colloids within the samples.

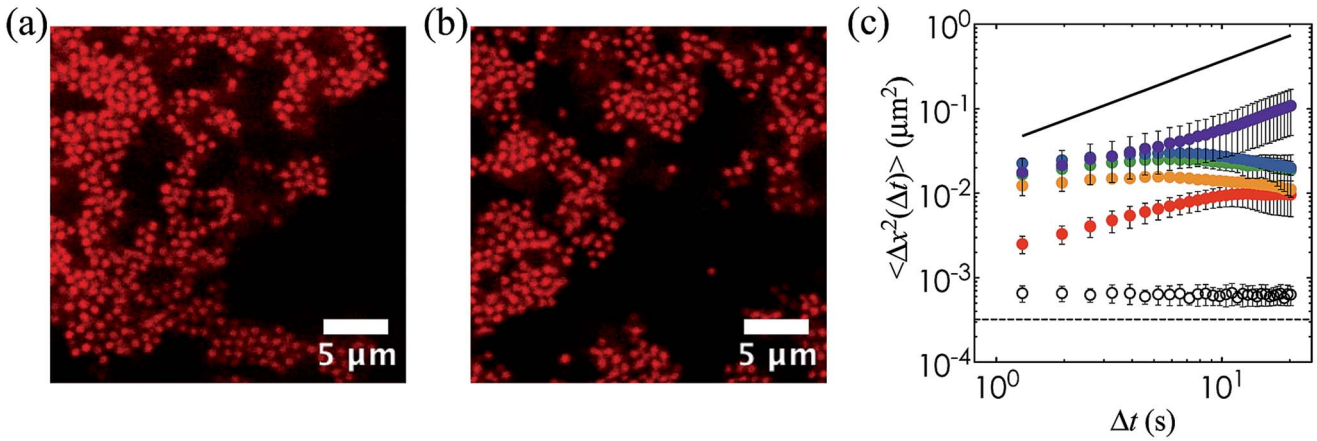

Fig. 1 Representative 2D confocal images of colloidal gels after applying (a) $\gamma = 0.6$ and (b) 80.0 at $\dot{\gamma} = 40\ s^{-1}$ in a shearing device. (c) Evolution of $\langle \Delta x^2 \rangle$ as a function of Δt from a completely arrested gel state (black open symbols) to a completely fluidized suspension (solid line), with the following applied deformations: $\gamma = 0.1$ (red), $\gamma = 0.6$ (orange), $\gamma = 6.0$ (green), $\gamma = 30.0$ (blue), and $\gamma = 80.0$ (purple). Dashed line represents the static noise level obtained from a photopolymerized sample. Error bars shown here are standard deviations from 3 independent measurements.

The emergence of a distinctive, shear-induced dynamical heterogeneity accompanies the increase in $\langle \Delta x^2(\Delta t) \rangle$ as a function of γ. The self-part of the van Hove correlation is computed from the colloidal trajectories and plotted for low, intermediate, and high γ at $\Delta t = 1.3$ s, 9.8 s, and 20.2 s in Fig. 2, so as to span the available dynamic range of the experiments. Free particles experiencing Brownian fluctuations exhibit a normal distribution in the van Hove self-correlation function:

$$G_s^g(\Delta x, \Delta t) = \sqrt{\frac{1}{2\pi\langle \Delta x^2(\Delta t)\rangle}} \exp\left[\frac{-\Delta x^2}{2\langle \Delta x^2(\Delta t)\rangle}\right] \quad (1)$$

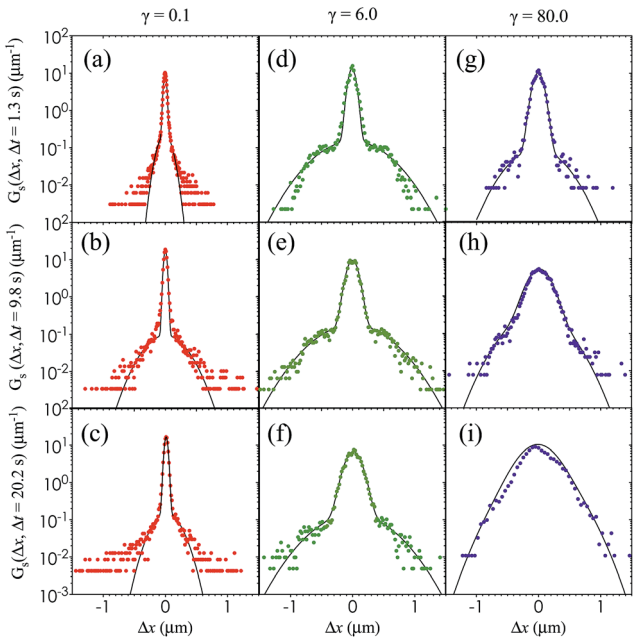

Fig. 2 Superimposed bimodal single particle displacement distributions of sheared colloidal gels showing slow and fast subpopulations. Gaussian distributions are fitted separately to the slow and fast subpopulations of particles, and the sum of the fits are plotted as solid lines. The self-part of the van Hove correlations are plotted for (a–c) $\gamma = 0.1$ (red), (d–f) $\gamma = 6.0$ (green), and (g–i) $\gamma = 80.0$ (purple). The distributions are shown for three different lag times: (a, d and g) $\Delta t = 1.3$ s, (b, e and h) $\Delta t = 9.8$ s, and (c, f and i) $\Delta t = 20.2$ s.

The variance of the distribution, σ^2, is related to the MSD through $\langle \Delta x^2(\Delta t) \rangle = \sigma^2$. Deviation from a Gaussian distribution in $G_s(\Delta x, \Delta t)$ signifies departure from free particle behavior. A narrow, non-Gaussian function is seen in ESI Fig. 1(f)† for quiescent gels at $\Delta t = 9.8$ s. The distribution is nearly independent of lag time, consistent with the particle localization that is characteristic of dynamical arrest in gels. Applying a step strain deformation results in superimposed bimodal distributions that are functionally distinct from the quiescent $G_s(\Delta x, \Delta t)$, as seen in Fig. 2(a)–(i). This bimodality indicates two subpopulations of particles with different MSD values.[3,23,33] Bimodal Gaussian fits are used to distinguish fast particles from slow particles based on the discontinuous slope in $G_s(\Delta x, \Delta t)$. Fig. 2 shows the overall contribution from the slow and fast colloids, plotted as the sum of bimodal Gaussian distributions separately fitted for both subpopulations. The value of $\Delta G_s(\Delta x, \Delta t)/\Delta x$ is computed for neighboring data points and a deviation of a factor of ten is assigned as the cutoff between slow and fast subpopulations. The width and the relative contributions of the two modes to the van Hove self-correlation functions increase considerably with both the step strain magnitude and the lag time. At the lowest applied strain of $\gamma = 0.1$, the values of $G_s(\Delta x, \Delta t)$ are relatively independent of Δt (Fig. 2(a)–(c)). At intermediate strain ($\gamma = 6.0$), Fig. 2(d)–(f) show that both distributions widen with increasing Δt. The time-dependent broadening in $G_s(\Delta x, \Delta t)$ is particularly apparent at the largest strain of $\gamma = 80.0$ (Fig. 2(g)–(i)). The distinction between slow and fast particles becomes small at large Δt (Fig. 2(i)), suggesting that the slow colloids exhibit much higher mobilities at large γ.

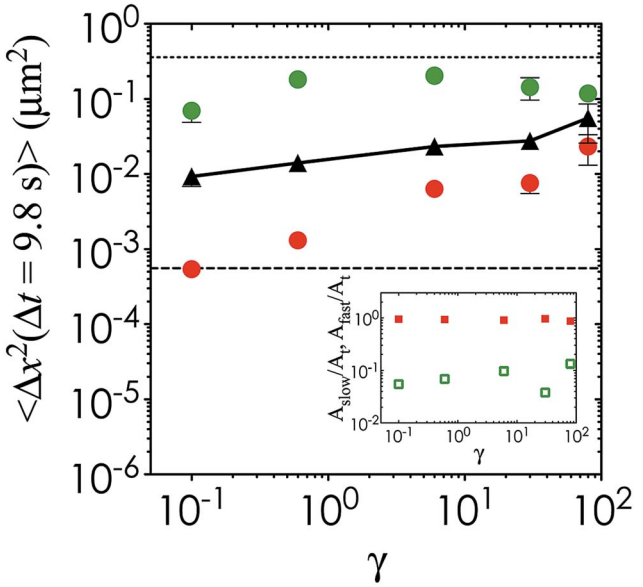

Fig. 3 MSD curves for the overall dynamics (black triangles) *versus* the slow (red circles) and fast subpopulation (green circles) of particles in sheared colloidal gels at $\Delta t = 9.8$ s. Error bars shown are standard deviations. A solid line is drawn through the overall dynamics to guide the eye. The free particle upper limit (dotted line) and the MSD of a quiescent gel (dashed line) are also shown. Inset: relative contribution of the slow (red filled circles) and fast (green open circles) colloids, quantified as the area under the distributions in Fig. 2, as a function of strain.

Because the distributions of both subpopulations are well represented by Gaussian functions, $G_s^g(\Delta x, \Delta t)$, the variances of the distributions (σ_{slow}^2 and σ_{fast}^2) are equivalent to the MSD of the subpopulations. We therefore separate the MSD values of fast and slow particles, $\langle \Delta x_{fast}^2(\Delta t)\rangle$ and $\langle \Delta x_{slow}^2(\Delta t)\rangle$, based on σ_{slow}^2 and σ_{fast}^2 and plot them in Fig. 3. The relative contributions of the slow and fast populations are quantified by the area under the two distributions, A_{slow} and A_{fast}, normalized by the total area A_t (Fig. 3, inset). The contribution of the fast subpopulation is small compared to the overall distribution. The displacement of fast particles remains approximately constant throughout all applied γ. Their mobility is about 40% of that expected for a free particle (Fig. 1(c)), suggesting that fast particles consist of free particles or very small clusters that diffuse rapidly. The mobility of the slow subpopulation increases with γ, with MSD values that increase by nearly two orders of magnitude between $\gamma = 0.1$ and $\gamma = 80.0$. This implies that slow colloids belong to the subpopulation that is most affected by the applied strain.

These combined observations suggest that strain-induced yielding of gels is accompanied by two dynamical changes. In the first change, which is already seen at $\gamma = 0.1$, the single dynamical population present in the colloidal gel bifurcates into subpopulations with fast and slow dynamics. The fast colloids displace nearly as free particles whereas the slow colloids have mobility that remains unchanged relative to the original quiescent population of colloids. The second change is seen as the strain is further increased, where the relative contributions of the fast and slow populations to the van Hove self-correlation function shifts toward the fast subpopulation. In addition, the mobility of the slow population itself increases as particles in this subpopulation become increasingly delocalized.

It is interesting to compare these observations about colloidal dynamics with previous studies of structural evolution upon yielding. These structural studies have shown that the contact number distribution in yielded gels changes with strain in a way that is consistent with the erosion of rigid clusters,[2,34] in which the abundance of high contact number colloids is depleted as strain is increased while the abundance of low contact number colloids increases. The remnant high contact number particles are sequestered in rigid, dense clusters and are responsible for the finite elastic modulus of yielded gels. These earlier measurements are in accord with the present work if the low contact number colloids from the structural measurements are identified with the fast subpopulation, and if the high contact number colloids are identified with the slow subpopulation. As the rigid clusters are eroded by the applied step stain, their size decrease and their mobility increase, consistent with the data shown in Fig. 2 and 3. Linking the structural and dynamic heterogeneity of yielded colloidal gels in this way has strong implications for the nonlinear elastic modulus of the gels, which we now explore through rheological measurements and application of mode coupling theory.

Accounting for dynamical heterogeneity in the microrheological prediction of the nonlinear elastic modulus

A particular form of MCT in which the gel structure factor is obtained from a two-component polymer interaction model

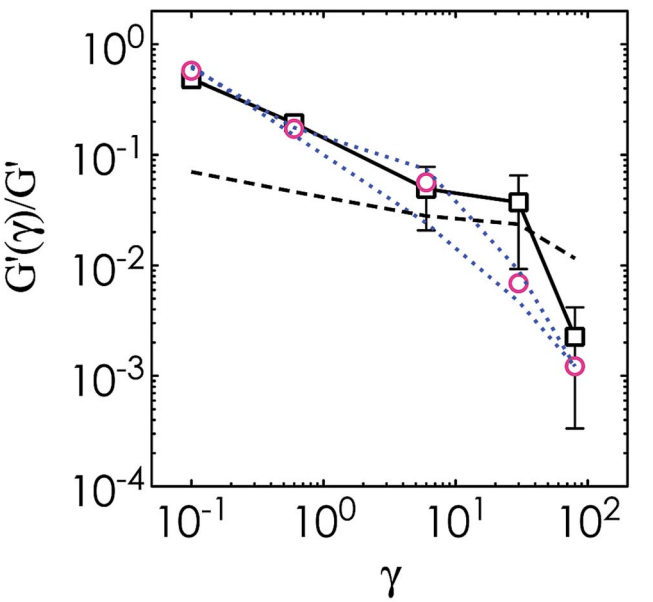

Fig. 4 Comparison of experimental elastic modulus (pink open circles) with high and low frequency bands (blue dotted lines) to theoretical predictions from MCT-PRISM (black dashed line). The modified MCT-PRISM predictions from eqn (3) are shown as open black squares joined by a solid black line. Error bars represent the range of predictions using four different values of the slow MSD (at Δt = 1.3, 4.5, 9.8, and 20.2 s) for each γ.

(PRISM) can be used to relate the zero-frequency strain-dependent elastic modulus, $G'_{micro}(\gamma)$, to the strain-dependent single-particle localization in the sample, $\langle \Delta r^2(\gamma) \rangle$:[19,20]

$$\frac{G'_{micro}(\gamma)(2a)^3}{k_B T} = 2.32 \frac{\phi a^2}{\langle \Delta r^2(\gamma) \rangle} \quad (2)$$

Here, $\langle \Delta r^2(\gamma) \rangle = 3\langle \Delta x^2(\gamma) \rangle$ is the mean-squared strain-induced localization length. The theoretical predictions are normalized by the static elastic modulus, $G'_{micro}(0)$, which is calculated from the mean-squared localization length of the quiescent gel shown in ESI Fig. 1(e).† Fig. 4 shows that the theoretical prediction for $G'_{micro}(\gamma)/G'_{micro}(0)$ deviates significantly from the experimental data, with underprediction at low strains and overprediction at high strains.

The strain-dependent localization length in eqn (2) is computed for an ensemble average of all colloids in the sheared gels. However, the dynamical heterogeneity shown in Fig. 2, combined with the nearly free-particle motion of the fast colloids in Fig. 3, suggest that the fast subpopulation does not contribute significantly to the nonlinear elastic modulus of the yielded gel. We therefore test a simple *ad hoc* revision of the MCT-PRISM in eqn (2) to reflect a case in which the contribution to elasticity arises only from the subpopulation of colloids that is slow and rigid. The modified expression predicts the nonlinear elastic modulus, $G'_{slow}(\gamma)$, by accounting for the strain-dependent volume fraction of structurally rigid clusters, $\phi_{rigid}(\gamma)$, in accordance to their slow dynamics, $\langle \Delta r_{slow}{}^2(\gamma) \rangle$, with the following relation:

$$\frac{G'_{slow}(\gamma)(2a)^3}{k_B T} = 2.32 \frac{\phi_{rigid}(\gamma) a^2}{\langle \Delta r_{slow}{}^2(\gamma) \rangle} \quad (3)$$

This expression consists of two components: (1) the localization length of the yielded gel is defined as that from the slow subpopulation of colloids from Fig. 3; (2) the volume fraction of colloids contributing to the nonlinear elasticity is taken as the high contact number subpopulation in the gel, compiled for the results of this work and of ref. 2 and plotted in ESI Fig. 3.† These values of $\phi_{rigid}(\gamma)$ are obtained by fitting a phenomenological stretched exponential function to samples used in ref. 2. The incorporation of $\phi_{rigid}(\gamma)$ into eqn (3) addresses the effect of rapid structural relaxation of the mobile subpopulation and provides an accurate depiction of the 3D structural landscape immediately after the cessation of flow. Ref. 2 found that the decrease in ϕ_{rigid} is a general function of γ for depletion gels ($0.375 \leq c/c^* \leq 1.1$) tested at large strain deformations ($0.5 \leq \gamma \leq 60$) and in the volume fraction range $0.10 \leq \phi \leq 0.20$. This range of conditions includes the gel of the present study. We further checked the consistency of this relation with the gels used in this study by a direct measurement of the value of ϕ_{rigid} at $\gamma = 6.0$ using the methods of ref. 2. We find that the measurement for this study agrees with the full correlation of ref. 2 to within experimental error (ESI Fig. 3†). The exponential fit of data in ESI Fig. 3† takes a compressed form of $\phi_{rigid}(\gamma) = 0.060 \exp[-(\gamma/35)^{1.5}]$ and is used in eqn (3).

We find that eqn (3), reflecting contribution from just the slow/rigid colloids, improves the agreement between theory and experiment (Fig. 4, solid line). This solid line, generated from eqn (3), represents the average of the time-dependent behavior ($\Delta t = 1.3$, 4.5, 9.8, and 20.2 s) of the slow MSD at different γ; its range is indicated by the error bars in Fig. 4. The largest improvement is seen at both low and high strains. At low applied strains, slow colloids are more localized than the full population, giving rise to an increased modulus prediction. The decrease in elastic modulus in the revised model at high strain is due to two effects: the slow subpopulation is highly delocalized, and the percentage of slow/rigid colloids contributing to the modulus is very small due to shear-induced cluster erosion. The combination of these factors is key to the improvement of theoretical predictions in Fig. 4.

We acknowledge certain limitations with our finding that the nonlinear rheology is correlated with the slow/rigid colloid populations in the gel. First, the waiting time imposed by residual flow at the largest applied strain ($\gamma = 80.0$) may have resulted in cluster reaggregation and slower dynamics than if measurements were taken immediately after the step strain application. Nevertheless, stress relaxation measurements show that this additional waiting time has a negligible effect on the shear modulus normalized by its linear value. Second, the nonlinear oscillatory measurements used for the rheological characterization represent a deformation that is different from the step strains applied in the microscopy experiments. Specifically, the step strain shear modulus decreases more rapidly from $\gamma = 0.1$ to 80.0 than the strain-dependent elastic modulus. Third, eqn (3) predicts the zero-frequency elastic modulus; however, the rheological measurements here are at a finite frequency and the microscopy studies are for a finite time interval. We averaged the time-dependent behavior of the dynamics of the slow colloids as well as the slight dependence of $G'(\gamma)$ on ω to address this point.

Despite these limitations, the present findings indicate that modifying the MCT-PRISM result for strain-dependent elasticity to include just the slow subpopulation of colloids in the gel improves the agreement between theory and experiment. This improvement is generated with no adjustable parameters in the comparison shown in Fig. 4, because all inputs to eqn (3) are available from direct experimental measurements.

Conclusions

In this work, we show that yielded colloidal gels display a distinctive form of dynamical heterogeneity involving two classes of particles. The dynamics of the fast subpopulation is similar to that of free particles. The slow subpopulation belongs to that of structurally rigid clusters that remain after the cessation of shear. These slow particles support the stress of the sheared gels. As the applied deformation is increased, the mobility of the slow subpopulation progressively increases. Our work points to the importance of incorporating strain-induced dynamical heterogeneity into theoretical models for the nonlinear rheological response of colloidal gels, and we use MCT-PRISM as an example of how microrheological models

might be modified to account for the slow subpopulation of stress-bearing colloids. This type of connection between strain-induced dynamical heterogeneity and nonlinear rheology could be drawn for a variety of dense colloidal systems with slow dynamics, for example in soft glasses[35] and in shear thickening fluids where hydrocluster formation is important.[36]

Acknowledgements

L.C.H., H.K., and M.J.S. acknowledge support from the National Science Foundation (NSF 0853648 and 1232937) and the International Fine Particles Research Institute (IFPRI). H.K. and K.H.A. acknowledge the support by the National Research Foundation of Korea (NRF) grant (no. 2013R1A2A2A07067387) funded by the Korea government (MEST).

References

1 C. P. Royall, S. R. Williams, T. Ohtsuka and H. Tanaka, *Nat. Mater.*, 2008, **7**, 556.
2 L. C. Hsiao, R. S. Newman, S. C. Glotzer and M. J. Solomon, *Proc. Natl. Acad. Sci. U. S. A.*, 2012, **109**, 160.
3 A. Puertas, M. Fuchs and M. Cates, *Phys. Rev. E: Stat., Nonlinear, Soft Matter Phys.*, 2003, **67**, 31406.
4 C. J. Dibble, M. Kogan and M. J. Solomon, *Phys. Rev. E: Stat., Nonlinear, Soft Matter Phys.*, 2006, **74**, 041403.
5 A. P. R. Eberle, N. J. Wagner and R. Castañeda-Priego, *Phys. Rev. Lett.*, 2011, **106**, 105704.
6 E. Zaccarelli and W. C. K. Poon, *Proc. Natl. Acad. Sci. U. S. A.*, 2009, **106**, 15203.
7 F. Sciortino, S. Mossa, E. Zaccarelli and P. Tartaglia, *Phys. Rev. Lett.*, 2004, **93**, 055701.
8 S. Ilett, A. Orrock, W. C. K. Poon and P. N. Pusey, *Phys. Rev. E: Stat. Phys., Plasmas, Fluids, Relat. Interdiscip. Top.*, 1995, **51**, 1344.
9 J. C. Conrad, H. M. Wyss, V. Trappe, S. Manley, K. Miyazaki, L. J. Kaufman, A. B. Schofield, D. R. Reichman and D. A. Weitz, *J. Rheol.*, 2010, **54**, 421.
10 M. Laurati, G. Petekidis, N. Koumakis, F. Cardinaux, A. B. Schofield, J. M. Brader, M. Fuchs and S. U. Egelhaaf, *J. Chem. Phys.*, 2009, **130**, 134907.
11 N. Koumakis and G. Petekidis, *Soft Matter*, 2011, **7**, 2456.
12 J. Bergenholtz and M. Fuchs, *Phys. Rev. E: Stat. Phys., Plasmas, Fluids, Relat. Interdiscip. Top.*, 1999, **59**, 5706.
13 E. Zaccarelli, G. Foffi, K. A. Dawson, S. V. Buldyrev, F. Sciortino and P. Tartaglia, *Phys. Rev. E: Stat., Nonlinear, Soft Matter Phys.*, 2002, **66**, 041402.
14 T. R. Kirkpatrick and P. G. Wolynes, *Phys. Rev. A: At., Mol., Opt. Phys.*, 1987, **35**, 3072.
15 Y. L. Chen and K. S. Schweizer, *J. Chem. Phys.*, 2004, **120**, 7212.
16 J. Bergenholtz, W. Poon and M. Fuchs, *Langmuir*, 2002, **19**, 4493.
17 H. Guo, S. Ramakrishnan, J. L. Harden and R. L. Leheny, *Phys. Rev. E: Stat., Nonlinear, Soft Matter Phys.*, 2010, **81**, 050401.
18 H. Guo, S. Ramakrishnan, J. L. Harden and R. L. Leheny, *J. Chem. Phys.*, 2011, **135**, 154903.
19 S. A. Shah, Y. L. Chen, K. S. Schweizer and C. F. Zukoski, *J. Chem. Phys.*, 2003, **119**, 8747.
20 V. Gopalakrishnan and C. F. Zukoski, *Langmuir*, 2007, **23**, 8187–8193.
21 S. Ramakrishnan, V. Gopalakrishnan and C. F. Zukoski, *Langmuir*, 2005, **21**, 9917.
22 C. J. Dibble, M. Kogan and M. J. Solomon, *Phys. Rev. E: Stat., Nonlinear, Soft Matter Phys.*, 2008, **77**, 050401.
23 Y. Gao and M. L. Kilfoil, *Phys. Rev. Lett.*, 2007, **99**, 078301.
24 A. Fall, J. Paredes and D. Bonn, *Phys. Rev. Lett.*, 2010, **105**, 225502.
25 P. Ballesta, R. Besseling, L. Isa, G. Petekidis and W. C. K. Poon, *Phys. Rev. Lett.*, 2008, **101**, 258301.
26 C. O. Klein, H. W. Spiess, A. Calin, C. Balan and M. Wilhelm, *Macromolecules*, 2007, **40**, 4250.
27 V. Kobelev and K. S. Schweizer, *J. Chem. Phys.*, 2005, **123**, 164902.
28 B. Chung, S. Ramakrishnan, R. Bandyopadhyay, D. Liang, C. F. Zukoski, J. L. Harden and R. L. Leheny, *Phys. Rev. Lett.*, 2006, **96**, 228301.
29 L. Mohan, R. Bonnecaze and M. Cloitre, *Phys. Rev. Lett.*, 2013, **111**, 268301.
30 P. J. Lu, E. Zaccarelli, F. Ciulla, A. B. Schofield, F. Sciortino and D. A. Weitz, *Nature*, 2008, **453**, 7194.
31 L. T. Shereda, R. G. Larson and M. J. Solomon, *Phys. Rev. Lett.*, 2008, **101**, 038301.
32 J. C. Crocker and D. G. Grier, *J. Colloid Interface Sci.*, 1996, **179**, 298.
33 W. K. Kegel and A. van Blaaderen, *Science*, 2000, **287**, 290.
34 J. D. Park and K. H. Ahn, *Soft Matter*, 2013, **9**, 11650.
35 A. Zaccone, H. Wu and E. Del Gado, *Phys. Rev. Lett.*, 2009, **103**, 208301.
36 N. J. Wagner and J. F. Brady, *Phys. Today*, 2009, **62**, 27.